

Enhancing sustainability of acid gas treatment in a Waste-to-Energy plant via Model Predictive Control

Riccardo Bacci di Capaci, Marco Vaccari*, Gabriele Pannocchia

University of Pisa, Department of Civil and Industrial Engineering, Largo Lucio Lazzarino 2, 56126 Pisa, Italy

ARTICLE INFO

Handling Editor: Panos Seferlis

Keywords:

Emission control
Model predictive control
MSW combustion
Process efficiency
Waste reduction

ABSTRACT

The municipal solid waste fed to waste-to-energy (WtE) plants produces acid flue gas with a wide and volatile range of composition, a scenario which implies significant process disturbances for traditional control schemes. In this paper, a two-stage dry sorbent system in an Italian treatment plant is used as a case study. The focus was on the first stage of abatement, where calcium hydroxide is injected into a reactor to reduce the hydrogen chloride (HCl) content in the acid flue gas. A state-space model, identified and tested in a previous work, was here implemented in a model predictive control (MPC) structure. In particular, four different MPC solutions were derived and tested on routine data in order to increase the process performance. Three suitable key performance indicators were used to assess the quantitative comparison between the proposed advanced control approaches and the simulated architecture of the one implemented in the WtE plant. The analysis evidenced the benefits obtained by MPC structures with respect to the current sub-optimal control architecture. Controller tuning and the possibility to include the online HCl concentration in the model have been also tested to highlight the best solution. Overall, the advanced controllers allowed one to achieve a solid profit-safety trade-off, by strictly tracking set-point on outlet HCl concentration and, at the same time, by requiring minimal sorbent doses and then minimal solid residues, with limited stress on the actuation system.

1. Introduction

One of the most impacting aspects of the environment linked to the global economy is the production of wastes (Makarichi et al., 2018). Even though municipal solid waste (MSW) accounts for only about 10% of total waste generated when compared with the data reported according to the European Union (EU) Waste Statistics Regulation (EU-Eurostat, 2021), its composition, distribution, and link to consumption patterns gives it a very high political profile. MSW generation and treatment in the EU from 1995 to 2020 show a very distinct trend towards less landfilling, as countries move steadily towards alternative ways of treating waste (EU-Eurostat, 2021, Table 2). In this framework, waste-to-energy (WtE) conversion technologies have received increasing attention in the last 20 years concerning improving waste management and sustainability (Putna et al., 2020).

Different studies have recently focused on developing sustainable WtE plants. Since many new WtE projects to safely manage MSW disposal are proposed every year, a specific tool that identifies and evaluates the risk factors affecting these projects' performance was recently proposed (Mousavi et al., 2021). Important criteria for the accurate selection of new projects are evaluated with a fuzzy risk-based decision model and its reliability was successfully tested in Iran.

Sustainability and economical optimization in terms of energy efficiency of WtE technologies are often considered together. Ni et al. (2022) have recently presented a waste heat recovery system, by combining a transcritical CO₂ system, an organic Rankine cycle (ORC), and a compression heat pump/refrigeration system. Exploiting multi-objective optimization to obtain the best working parameters, the proposed WtE plant retrofit reveals a huge potential for waste heat recovery and provides a strategy to reduce energy consumption as well as improve economic and environmental performance. Iqbal and Kang (2021) focused on converting waste into profit, reducing environmental pollution, and generating energy from bio-waste by optimizing the supply chain of two plants: the waste collector center and a biogas production plant. The biogas is used to fulfill the WtE plant energy requirements and the excess amount is sold in the market for profit. Another novel high-efficiency WtE power plant uses refuse-derived fuel as feedstock by integrating torrefaction pretreatment, including plasma gasifier, solid oxide fuel cell, and combined heat and power system (Kuo et al., 2021). The two different scenarios studied differ in the presence of a CO₂ capture system, and the authors show that the capture and compression processes account for an energy penalty of about 6%.

* Corresponding author.

E-mail addresses: riccardo.bacci@unipi.it (R. Bacci di Capaci), marco.vaccari@ing.unipi.it (M. Vaccari), gabriele.pannocchia@unipi.it (G. Pannocchia).

<https://doi.org/10.1016/j.jclepro.2023.137222>

Received 24 January 2023; Received in revised form 20 March 2023; Accepted 17 April 2023

Available online 22 April 2023

0959-6526/© 2023 The Authors. Published by Elsevier Ltd. This is an open access article under the CC BY license (<http://creativecommons.org/licenses/by/4.0/>).

Nomenclature

Acronims

PB	Proportional Band
TI	Integral time constant
ARMAX	AutoRegressive-Moving-Average with eXogenous inputs (model)
ARX	AutoRegressive with eXogenous inputs (model)
DCS	Distributed Control System
FFT	Feed-Forward control with Feedback Trim
MPC	Model Predictive Control
MSW	Municipal Solid Waste
PI	Proportional-Integral
SMPi	Sample Measurement Point number i
SS	State-Space
WtE	Waste-to-Energy

Symbols

A, B, C	Matrices of the identified model
C_{HCl}^i	Concentration of HCl at point i
d	Model disturbance
MV	Manipulated Variable
Q, S, R, Q_N	Weight matrices of the optimal control problem
$Q_{\text{Ca(OH)}_2}$	Mass flow rate of Ca(OH)_2
u	Model input
x	Model state
y	Model output

Superscripts

-	Optimal steady-state values
^	Estimated quantity
*	Optimal state estimate
*	Optimal dynamic solution
+	Related to the next time step

Subscripts

d	Related to the disturbance model
i	Related to the chemical compound $i = \text{HCl}, \text{Ca(OH)}_2$
k	Iteration in the MPC algorithm
m	Related to the measurable disturbance
sp	Set-point values
FB	Feedback
FF	Feed-Forward

In general, the emission composition from WtE systems varies from time to time depending mainly on the type of municipal waste treated by the plant (Pavlas et al., 2010). As a consequence, also the content of acid elements (as HCl, SO_2 , HF) in the combustion flue gas is affected by this fluctuation. As an example, the emission and capture characteristics of HCl during PVC and food waste combustion in CO_2/O_2 atmospheres were recently investigated in (Dai et al., 2020). Results showed that the capacity of limestone sorbents of absorbing HCl decreases with the increase of temperature by few percentage points and that this efficiency could be improved by the addition of NaOH. Among best available techniques used for acid gas removal, many methods indeed imply the direct injection of sorbent in the furnace as a primary deacidification stage (Dal Pozzo et al., 2018a). It is to be noted

that when acting to comply with strict standards of emission, the use of a large excess of reactants with respect to the stoichiometric demand is the typical approach (Dal Pozzo et al., 2021). This solution indeed ensures to neutralize with confidence the acid gases and avoids any overshoot in emissions at the stack, but the economic aspect linked to the cost of basic sorbents is often totally neglected. As a matter of fact, feeding an excess of reactant translates also into the production of solid process residues, therefore representing a significant source of indirect environmental impacts (Biganzoli et al., 2015).

To identify the techno-economic optimum in this safety-profit trade-off, a recent study developed a data-driven phenomenological model linking HCl and SO_2 conversion to reactant feed rate (Dal Pozzo et al., 2020). This model showed a reduction of the total operating costs for one-stage treatment WtE plants and high SO_2 concentration in the flue gas. Another model to estimate HCl and SO_2 emissions in a WtE plant flue gases to best manage sorbents feed rate is based on material flow analysis (Zhang et al., 2019). Monitoring the pollutants concentrations in the full-scale plant estimations showed to be more reliable when based on the amounts of chlorine and sulfur in the air pollution control residues gas rather than in the original waste fed to the plant.

With increasingly stringent emission standards, optimizing the feed of reactants without reducing the pollutant abatement performance is a crucial problem to be solved. In this sense, advanced control systems play a key role in meeting this goal for this class of industrial processes (Li et al., 2020). Several are indeed examples of advanced process control, mainly model predictive control (MPC), applied to process industry in order to manage pollutant emissions.

A network MPC has been recently presented to assess the environmental and technical performance of a depropanizer column (Shin et al., 2020). The implementation of the proposed MPC structure showed to increase the robustness of the control system ensuring both high product quality, and a reduction in terms of energy consumption and pollutants emissions. Another process control strategy based on Deep Neural Network MPC has optimized the management of the denitration system and reduced the amount of pollutant emissions in the cement calcination process (Xu et al., 2022). Compared with traditional controllers (e.g., PID), experimental results showed that the proposed MPC scheme has higher robustness in controlling the NOx emission by reducing at the same time the reactant feed. With a similar goal, by using a gain scheduling model, an MPC strategy has been able to reduce NOx flue gas concentration by two-thirds and reagent consumption by 25%, also avoiding additional unreacted pollutant emission of a selective catalytic reduction in a coal-fired power plant (Zhang et al., 2018b). In the context of wastewater treatment plant management, an application of MPC was studied for performance assessment of the simultaneous removal of nitrogen and phosphorus with an activated sludge model (Shiek et al., 2021). On the other hand, the production efficiency of a bioethanol plant was increased by adopting a multi-stage offset-free nonlinear MPC by revealing how the controller sampling time is crucial in the presence of parameter uncertainties (Skupin et al., 2022). When considering flue gas treatment units, a recent review of methods for modeling and controlling solvent-based post-combustion CO_2 capturing processes evidenced the importance of designing suitable approaches as the key to meeting operational tasks given the dynamic characteristics of the process (Wu et al., 2020). For a more complete understanding of the critical aspects linked to MPC solutions applied to post-combustion capture processes, the reader can refer to Wu et al. (2020, Table 4) and the works therein. Different MPC structures have been analyzed and compared in details; for example: linear (Hosseini Sahraei and Ricardez-Sandoval, 2014), multi-model (Wu et al., 2018), nonlinear (Zhang et al., 2018a), and economic MPC (Chan and Chen, 2018).

Increasingly stringent environmental regulations and growing demands for higher energy efficiency, have also brought MPC technologies inside WtE plants (Leskens et al., 2005). This has improved the performance of the combustion processes on one side, and of the flue

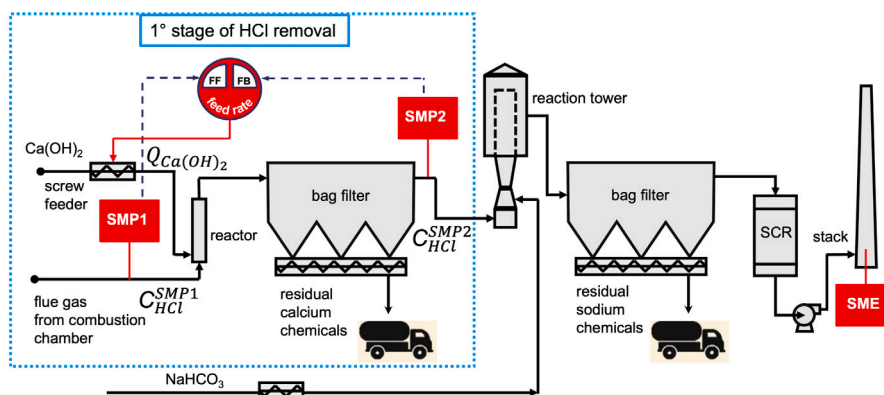


Fig. 1. The two-stage gas abatement line of the WtE plant under study, with the control architecture for the first stage.
Source: Adapted from Dal Pozzo et al. (2021).

gas cleaning equipment on the other, showing robustness on stationary stochastic disturbances of relatively small amplitude. By using linear regression models and multiscale convolutional neural networks, Bigoni et al. (2021) developed a data-driven model for designing an MPC framework. The control strategy was successfully integrated into a real online WtE facility by fulfilling multi-constraint requirements such as energy demand, safety ranges of working conditions, and emission of uncombusted and polluting fumes. Nonetheless, when measuring pollutant emission is not possible or even not economically feasible, developing models to be implemented in model-based control technologies to assess emission monitoring and check regulatory compliance can also require the involvement of rigorous process simulators (Vaccari et al., 2020) or more complex tools (Dal Pozzo et al., 2023).

For the case investigated in the present work, the difficulty to be addressed is the HCl content in the flue gas which can be really oscillating over time, because of the variable composition of the MSW burnt into WtE facility (Dal Pozzo et al., 2021). Many WtE plants employ a two-stage system for removing acid gases, in which firstly hydrated lime is dosed, and after sodium bicarbonate is injected. In addition to the already mentioned performance flaws in the use of sorbent excess, there is also a practical issue linked to the variability in the concentration of HCl exiting the first stage, since this stream acts as an input disturbance in the subsequent second stage of abatement. Hence, to manage both these aspects, suitable dynamic data-driven models of the first gas abatement unit of a WtE facility exploiting standard systems identification methods and input–output routine operation data were recently developed (Bacci di Capaci et al., 2022).

Therefore, the main objective of the present paper is to design and compare different types of model predictive controllers so that to improve acid gas treatment management. Such enhanced control formulations are based on the dynamic models identified and validated in our previous work (Bacci di Capaci et al., 2022). In this way, we here present a detailed comparison of MPC formulations with a realistic simulation of the traditional control architecture implemented in the Distributed Control System (DCS) of the considered WtE facility. To the best of our knowledge, no MPC formulation is available in the literature for the specific system considered, that is, the flue gas treatment line of a waste-to-energy plant by using solid alkaline sorbents. Similar solutions of MPC concern the optimization of WtE facilities in terms of energy cost and utility demand. The organization of the paper is as follows: the investigated removal unit with the corresponding control system is described in Section 2; the proposed advanced control architecture is illustrated in Section 3. Main results in terms of performance comparison are then discussed in Section 4; finally, Section 5 summarizes the conclusions of the work.

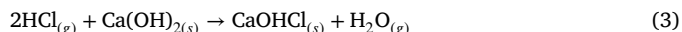
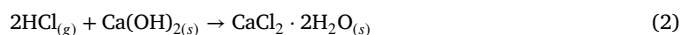
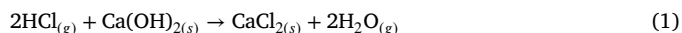
2. Case study definition

This section illustrates the main characteristics of the considered industrial system, that is, the dry sorbent injection process and the related control system.

2.1. Dry sorbent injection

The WtE plant considered in this paper is a medium-sized facility operating in Northern Italy. The plant is characterized by a standard two-stage acid gas abatement unit with alkaline dry sorbent injection, and is comprised of a step of reaction and then filtration taking place at ≈ 180 °C (see Fig. 1). Calcium hydroxide ($\text{Ca}(\text{OH})_2$) is firstly injected to a tubular reactor; then, sodium bicarbonate (NaHCO_3) is fed into a reaction tower. Two baghouse filters operated by reverse pulse jet cleaning are used to separate unreacted sorbent and residual solid chemicals: i.e., blasts of compressed air break the cake deposited on filter tissues. Flue gas composition is measured by three sensors placed at different points of the line: at the combustion chamber outlet (SMP1), after the first baghouse (SMP2), and at the stack base (SME). Various acid components are present in the flue gases: in decreasing order of concentration, HCl, NO, SO_2 , HF, NO_2 are typically revealed (Dal Pozzo et al., 2021).

The focus of this study is on the first stage of abatement, as highlighted in Fig. 1. Different acid–base reactions occur in this first step; the most critical are the ones involving the abatement of hydrogen chloride. In particular, three gas–solid reactions are considered in most of the kinetics modeling studies (Dal Pozzo et al., 2018b):



Significant amount of solid calcium chemicals are indeed produced by the previous set of reactions: anhydrous (CaCl_2) and dihydrate ($\text{CaCl}_2 \cdot 2\text{H}_2\text{O}$) calcium chloride, and calcium hydroxy chloride (CaOHCl). These materials form an inert cake as they easily get deposited over the tissue of the baghouse.

2.2. The present control system

The control logic implemented in the plant DCS receives the variables measured online and, for the first stage of abatement, manages the regulation of $\text{Ca}(\text{OH})_2$ feed rate. As with most WtE plants, the control system implemented is designed to add a large amount of solid sorbent that exceeds the stoichiometric value. This approach guarantees a safe abatement and then ensures emission limits measured at the stack to be respected, limits which are particularly low for HCl emission in

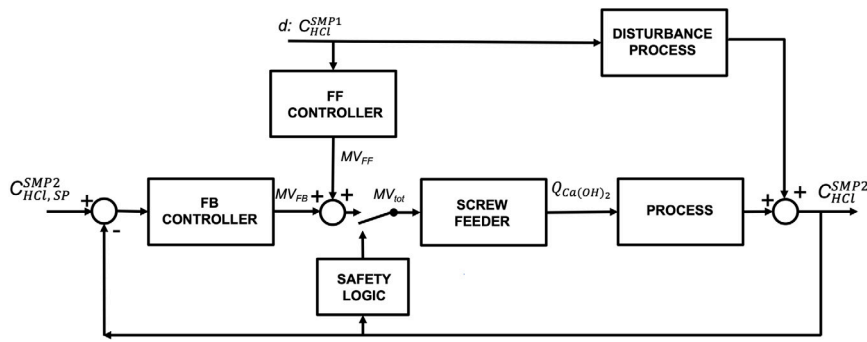


Fig. 2. Scheme of the FFT, the implemented control system for the first stage of abatement.

WtE plants. Nevertheless, large amount of solid residuals are produced, which then imply a high cost of disposal (Dal Pozzo et al., 2021).

In detail, the control architecture is comprised of a feed-forward control with feedback trim (FFT), as shown in Fig. 2: the outlet concentration of hydrogen chloride (C_{HCl}^{SMP2}) is the controlled variable, expressed in mg/Nm^3 , measured at SMP2; the mass flow rate of calcium hydroxide ($Q_{Ca(OH)_2}$) is the manipulated variable, expressed in kg/h ; inlet concentration of HCl (C_{HCl}^{SMP1}) acts as a process disturbance, measured at SMP1. This control solution is suited for such a scenario, where the rejection of external disturbances is of primary importance. Besides the traditional feedback control loop, the feed-forward element is indeed able of undertaking a preventive control action against the most critical disturbance: the amount of HCl entering the reactor.

As shown in Fig. 2 and in Eq. (4), in the FFT architecture the manipulated variable (MV_{tot}) is given by the sum of the control action from two controllers: feedback (FB) and feed-forward (FF).

$$MV_{tot} = MV_{FB} + MV_{FF} \quad (4)$$

In particular, the feed-forward action of the controller implemented in the DCS is:

$$MV_{FF} = CK(VN + CB) \quad (5)$$

where parameter CK is a compensation gain with respect to the feed-forward component VN , possibly added to a constant bias CB . Note that these additional tuning parameters (CK , CB) can increase/decrease the feed-forward action of FFT to quickly manage non-ordinary operation scenarios, as start-up, shut-down, and equipment tests. As feed-forward component VN , a proportionality relation between input HCl load and calcium hydroxide dosage is adopted. The standard control tuning imposes $CK = 1$ and $CB = 0$, and VN is set equal to:

$$VN = \left(\frac{1}{2} \cdot \frac{Q^{SMP1} \cdot C_{HCl}^{SMP1}}{MW_{HCl}} \right) \cdot r_s \cdot \frac{MW_{Ca(OH)_2}}{R_{sf}} \quad (6)$$

where the product of the flue gas flow rate (Q^{SMP1}) and the inlet concentration of HCl, (C_{HCl}^{SMP1}) yields the mass flow rate of HCl entering the reactor. Note that the term in parenthesis represents the stoichiometric requirement of $Ca(OH)_2$ necessary to treat such acid gas mass flow; MW_i is the molecular weight of the substance i , and r_s is the excess factor, which indeed represents the tuning parameter of the feed-forward component. Finally, R_{sf} is a proportionality coefficient between the mass flow rate of dosed $Ca(OH)_2$ and the actual manipulated variable, that is, the speed of rotation of the screw feeder, scaled as percentage of the max value.

As a feedback component, a standard proportional-integral (PI) velocity algorithm is employed:

$$MV_{FB,k} = MV_{FB,k-1} + PB \cdot (e_k - e_{k-1}) + \frac{PB \cdot T_s}{TI} e_k \quad (7)$$

where $e_k = C_{HCl,k}^{SMP2} - C_{HCl,sp}^{SMP2}$ is the control error; PB is the proportional band, TI the is integral time constant; $T_s = 1$ min is the controller sampling time and k is the generic time step.

Finally, an additional level of safety on the FFT logic is superimposed (see Fig. 2). If the outlet HCl concentration exceeds a preset threshold, the sorbent dosage is forthwith set to its maximum value ($Q_{Ca(OH)_2} \approx 318$ kg/h), that is, a percentage command of 80% until the outlet HCl concentration returns below the threshold. As an example, the time trends of the considered variables of the first stage of abatement, registered for three consecutive h, are reported in Fig. 3. The set-point of outlet HCl concentration is set to 450 mg/Nm^3 ; several spikes on $Ca(OH)_2$ feed rate are observed due to the aggressive action of the feed-forward component and the safety logic.

3. Methodology

In this section, the phases of the design of an advanced model-based controller, capable of significantly improving process operation and economic performance, are illustrated. With such a controller, it is indeed possible to achieve a suitable safety-profit trade-off, by optimizing emission levels and minimizing solid sorbents and residuals.

3.1. Model identification

It is well-known that the project of an advanced controller passes through the identification of an accurate process model as the first step.

The open-source Systems Identification Package for PYthon (SIPPY) (Armenise et al., 2018) was used in this work to obtain dynamic models to describe the first abatement stage of the analyzed WtE plant. Input-output data collected from suitable plant tests were employed; in particular, two data sets were collected for the model identification purpose, while the other two data sets were gathered for the consequent model validation. A set of 2×1 systems were identified and then validated. In particular, the two considered inputs are the concentration of HCl measured at SMP1 and expressed in mg/Nm^3 (C_{HCl}^{SMP1}), and the mass flow rate [kg/h] of $Ca(OH)_2$ ($Q_{Ca(OH)_2}$); the process output is the HCl concentration measured at SMP2, and still expressed as mg/Nm^3 (C_{HCl}^{SMP2}).

As already anticipated, a disturbance variable is represented by the inlet concentration of HCl, which is related to the composition of the solid waste fractions burnt in the combustion chamber; on the opposite, a standard manipulated variable is the flow rate of $Ca(OH)_2$, which can be indeed varied by the operators in the control room. During the plant data collection, the control system, that is, the FFT architecture of Fig. 2, was partially deactivated and two different sequences of Generalized Binary Noise were defined as system inputs; this type of experiments represent suitable tests to identify the process dynamic. We then considered and compared different linear model structures and orders. Among input-output models, AutoRegressive and AutoRegressive-Moving-Average with eXogenous inputs models, that is, ARX and ARMAX structures, were tested. Further details of this analysis are here omitted for the sake of brevity, and can be found in our preliminary work (Bacci di Capaci et al., 2022). On the other hand, our

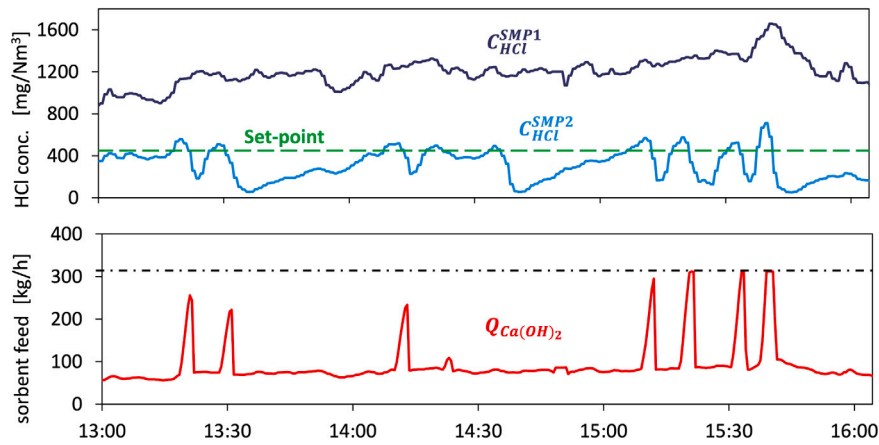


Fig. 3. Registered variables of the first stage of abatement at points SMP1 and SMP2. Source: Adapted from Dal Pozzo et al. (2021).

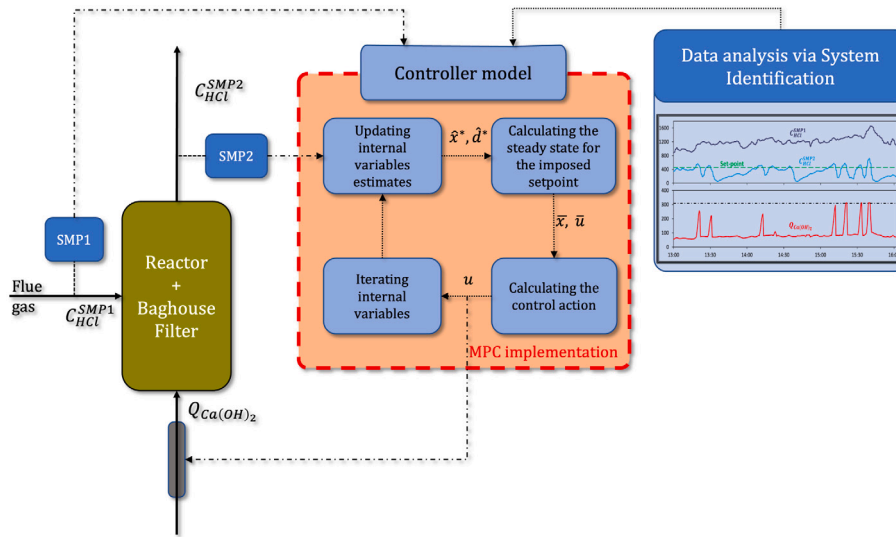


Fig. 4. Scheme of offset-free MPC implementation proposed.

present focus is on the state-space (SS) structures, which are typically implemented in MPC algorithms.

As SS model, the *process form* was considered:

$$\begin{cases} x^+ = Ax + Bu \\ y = Cx \end{cases} \quad (8)$$

where $y \in \mathbb{R}^{n_y}$, $x \in \mathbb{R}^{n_x}$, $u \in \mathbb{R}^{n_u}$ are the system output, state, input; x^+ indicates the state at the following time step (i.e., $k + 1$); $A \in \mathbb{R}^{n_x \times n_x}$, $B \in \mathbb{R}^{n_x \times n_u}$, $C \in \mathbb{R}^{n_y \times n_x}$ are the system matrices.

A well-established subspace method with a so-called parsimonious algorithm (known as PARSIM-K) was considered as identification method (Pannocchia and Calosi, 2010). In the present case, the dimension of the identified model are $n_u = 2$, $n_y = 1$, $n_x = 4$, this latter obtained after a suitable optimization procedure as described in Bacci di Capaci et al. (2022).

3.2. Adopted MPC controller

In this section the MPC formulation adopted for controlling the outlet HCl flow rate, which exploits the state space model previously identified, is described. Fig. 4 shows the structure of the offset-free MPC implementation proposed.

As seen in the previous section, the controller model is built using system identification on trends of data appositely collected on the

variables of interest. In addition to that, and to reach the offset-free performance, the considered formulation adopts an additional internal variable representing a disturbance model, thus augmenting the plant model in Eq. (8) into the following structure:

$$\begin{aligned} x^+ &= Ax + Bu + B_d d \\ d^+ &= d \\ y &= Cx + C_d d \end{aligned} \quad (9)$$

in which $d \in \mathbb{R}^{n_d}$ is the so-called *disturbance*, where selecting $n_d = n_y$ has proven to effectively improve the MPC performances under plant-model mismatch (Pannocchia, 2015). The effects of such a disturbance on the state and output are modeled via the two additional matrices $B_d \in \mathbb{R}^{n_x \times n_d}$ and $C_d \in \mathbb{R}^{n_y \times n_d}$. As depicted in Fig. 4, every sample time the current output measurement C_{HCl}^{SMP2} is used to update the internal variables estimates (x and d) computed at the previous iteration. Different types of state estimators have been proposed throughout the history of predictive control and MPC, in particular. The most common and established methods consist of filtering the predicted quantities by using the current measurement (y_k) and a proper weight matrix, constant (i.e., Luenberger observer) or varying over time (i.e. Kalman filter) (Auger et al., 2013). For the purpose of this work, the internal variable estimates are updated using a Kalman filter-like, so that the

new values are evaluated as follows:

$$\begin{aligned} \hat{x}_k^* &= \hat{x}_k + K_{k,x}(y_k - \hat{y}_k) \\ \hat{d}_k^* &= \hat{d}_k + K_{k,d}(y_k - \hat{y}_k) \end{aligned} \quad (10)$$

in which $K_k = \begin{bmatrix} K_{k,x}^T & K_{k,d}^T \end{bmatrix}^T$ is the filter gain matrix $\in \mathbb{R}^{(n_x+n_d) \times n_y}$, updated every sample time, and $\hat{x}_k, \hat{d}_k, \hat{y}_k$ are the predicted values evaluated by using the augmented model (9). The quantity $y_k - \hat{y}_k$ is called the prediction error and defines the gap between the predicted concentration of HCl at SMP2 defined by model (9) and the real measurement at each time k .

The new internal variables estimates are then fed into an optimization problem to calculate the steady-state conditions that minimize the distance from the desired external set-points (u_{sp}, y_{sp}) while respecting the imposed constraints (e.g bound constraints on states, inputs and outputs and model dynamics fulfillment). Specifically, the optimization problem solved is the following:

$$(\bar{x}_k, \bar{u}_k, \bar{y}_k) = \arg \min_{x,u,y} (y - y_{sp})^T \bar{Q}(y - y_{sp}) + (u - u_{sp})^T \bar{R}(u - u_{sp})$$

s.t.: system in (9) with $d = \hat{d}_k^*$ and bounds on optimization variables (11)

The quadratic objective function allows an easy tuning of the desired outcomes, that is addressing more the C_{HCl}^{SMP2} set-point or the one for $Q_{Ca(OH)_2}$, by changing the values of $\bar{Q} \in \mathbb{R}^{n_y \times n_y}$, the output penalty matrix, and $\bar{R} \in \mathbb{R}^{n_u \times n_u}$ the control penalty matrix.

Therefore, with the updated estimates of the internal variables and the computed steady-state triple $(\bar{x}_k, \bar{u}_k, \bar{y}_k)$, the new control action, that is the new value of the calcium hydroxide flow rate, is computed with a dynamic optimization problem. The goal of such problem is to find the optimal trajectory (x, u) from the current state and input to the targets of Problem (11) over a prediction horizon N steps long as follows:

$$\begin{aligned} (x_k^*, u_k^*) &= \arg \min_{x,u} \sum_{i=0}^{N-1} [(x_i - \bar{x}_k)^T Q(x_i - \bar{x}_k) + \Delta u_i^T S \Delta u_i] \\ &+ (x_N - \bar{x}_k)^T Q_N(x_N - \bar{x}_k) \end{aligned} \quad (12)$$

subject to

$$\begin{aligned} x_0 &= \hat{x}_k^* \\ x_{i+1} &= Ax_i + Bu_i + B_d \hat{d}_k^* \\ y_i &= Cx_i + C_d \hat{d}_k^* \\ c_{bnd,dyn}(x_i, u_i, y_i, \Delta u_i) &\leq 0 \end{aligned}$$

where $Q \in \mathbb{R}^{n_x \times n_x}$, and $S \in \mathbb{R}^{n_u \times n_u}$ are the state, and control difference penalty matrices respectively; $c_{bnd,dyn}(x_i, u_i, y_i, \Delta u_i)$ are bound constraints for the dynamic problem, not necessarily equal to the one in Problem (11); $\Delta u_i = u_i - u_{i-1}$ is the input rate of change, and, finally, $Q_N \in \mathbb{R}^{n_x \times n_x}$ is the terminal weight penalty matrix.

Alternatively, another tuning option can be adopted thus modifying the objective function of Problem (12) as follows:

$$\begin{aligned} (x_k^*, u_k^*) &= \arg \min_{x,u} \sum_{i=0}^{N-1} [(x_i - \bar{x}_k)^T Q(x_i - \bar{x}_k) + \\ &(u_i - \bar{u}_k)^T R(u_i - \bar{u}_k) + \Delta u_i^T S \Delta u_i] + (x_N - \bar{x}_k)^T Q_N(x_N - \bar{x}_k) \end{aligned} \quad (13)$$

which includes also the control penalty matrix $R \in \mathbb{R}^{n_u \times n_u}$. Usually, this second option is less frequently adopted in industrial applications because it makes the controller more performing in reaching the desired set-points but also more aggressive and thus possibly causing mechanical stress on the actuation system. In our case, in which the concentration of HCl in the flue gas is particularly fluctuating, and therefore steady-state conditions of such disturbance are difficult to reach, this could lead to a much faster deterioration of the sorbent feeding system implying a consequent raise in maintenance costs. In

any case, the current control action is selected as the first component of the optimal sequence u_k^* :

$$u_k = u_k^*[1] \quad (14)$$

This is then sent to the process to update the set-point value of $Q_{Ca(OH)_2}$ and at the same time to the controller model to update the internal variables and therefore retain the memory effect of previous iterations.

3.3. Measurable disturbance

As anticipated, the modeling of the studied process, and in particular the controlled variable, that is, the outlet concentration of HCl (C_{HCl}^{SMP2} in Fig. 1) is highly affected by the variability of HCl entering the reactor (C_{HCl}^{SMP1}), which strictly depends on the MSW content fed to the plant (Dal Pozzo et al., 2021). As also depicted in Fig. 4, including C_{HCl}^{SMP1} in the controller model would benefit its performance. Nevertheless, such a disturbance is registered at SMP1, hence falling into the so-called category of *measurable disturbances*. Therefore, Fig. 5 depicts how the controller model is updated using the online measurement of C_{HCl}^{SMP1} . These disturbances are peculiar since, although they cannot be manipulated to control the output variables for the intended interests, they can be treated as input variables for their effect on the outputs, and therefore they are comprised in the model identification stage.

For such reason, from a modeling point of view, the measurable disturbances d_m influence the output variables in a similar way as for the manipulated variables, but through a separated specific dynamic B_m . In this sense, the identified SS model in (8) becomes:

$$\begin{aligned} x^+ &= Ax + \tilde{B}\tilde{u} & \rightarrow & \quad x^+ = Ax + Bu + B_m d_m \\ y &= Cx & & \quad y = Cx \end{aligned} \quad (15)$$

in which $\tilde{B} = \begin{bmatrix} B & B_m \end{bmatrix}$ and $\tilde{u} = \begin{bmatrix} u^T & d_m^T \end{bmatrix}^T$.

We underline that modeling such measured disturbances is different from augmenting the model adopted in the MPC, as shown in (9). In fact, the disturbance model d is designed to tackle two main problems that can affect the MPC performances: the plant-model mismatch and unmeasured disturbances. Hence, in principle, one can speculate that not considering the B_m dynamic in (9) still fit in the plant-model mismatch case, and so the disturbance model alone can cover such deficiency. Such a statement is true, but not complete. In fact, considering the feedback behavior of the controller together with the plant dynamics, the measured disturbances registered at time k ($d_{m,k}$) affect the output at the next time step $k + 1$, while the disturbance model estimate \hat{d}_k^* is calculated to assess the discrepancy between \hat{y}_k and y_k . This would then translate into a systematic one-step delay of the control action sent to the plant. Note that results presented in Section 4 demonstrate such difference in MPC formulations.

For this reason and for consistency with the process model identified in (15), the augmented model used in the MPC algorithm described in Section 3.2 becomes the following:

$$\begin{aligned} x^+ &= Ax + \tilde{B}\tilde{u} + B_d d & \quad x^+ &= Ax + Bu + B_m d_m + B_d d \\ d^+ &= d & \rightarrow & \quad d^+ = d \\ y &= Cx + C_d d & & \quad y = Cx + C_d d \end{aligned} \quad (16)$$

4. Numerical results and discussion

The considered control systems are here analyzed and compared on the same set of routine plant data. In particular, a data window of 15 h with $T_s = 1$ min is considered, which corresponds to $N_s = 900$ time samples.

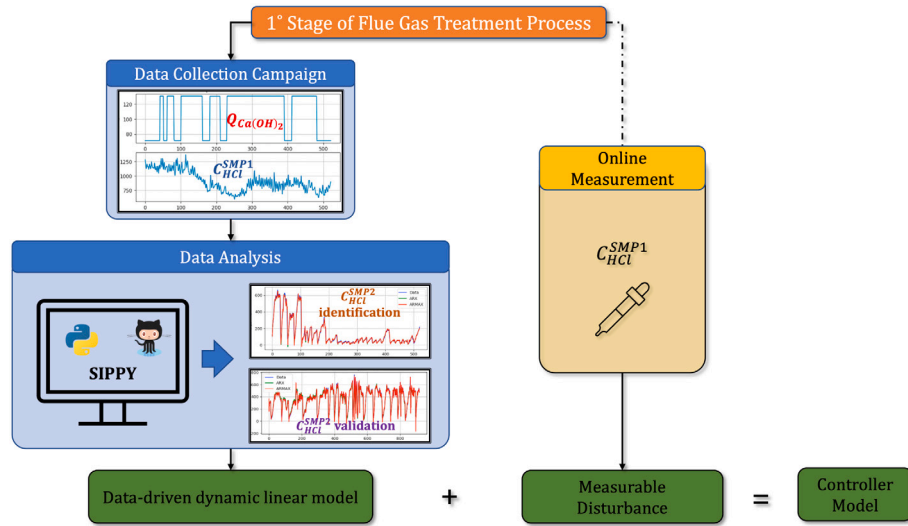


Fig. 5. Controller model implementation scheme: data-driven analysis using SIPPY (Armenise et al., 2018) plus online measurement.

4.1. The compared scenarios

The control architecture of the first stage of the considered gas removal line is simulated as in Section 2.2, and four different formulations of MPC are investigated. In particular, two different objective functions for the dynamic module are tested, and the effect of input HCl concentration (C_{HCl}^{SMP1}) as measurable disturbance is evaluated. In details:

- MPC1: for which the standard problem of (12) is adopted, and input HCl concentration is not used as measurable disturbance;
- MPC1-md: the same problem of (12) is adopted, and C_{HCl}^{SMP1} is considered as measurable disturbance;
- MPC2: the modified problem of (13) is used, and C_{HCl}^{SMP1} is not exploited;
- MPC2-md: the modified problem of (13) is adopted, and C_{HCl}^{SMP1} is considered within the model.

The identified model. The same state-space model is identified and used in all scenarios for closed loop simulation of the process to be controlled. The following 2×1 model – with four states, that is, $n = 4$ – is considered (Bacci di Capaci et al., 2022):

$$\begin{aligned}
 A &= \begin{bmatrix} 0.93576809 & 0.31692353 & -0.08834079 & 0.16453699 \\ -0.07693767 & 0.8920683 & -0.15241918 & -0.07328362 \\ -0.13400886 & 0.19861726 & 0.89859242 & -0.27425192 \\ -0.36173905 & -0.06163486 & 0.42074865 & 0.43828749 \end{bmatrix}, \\
 \tilde{B} = [B \quad B_m] &= \begin{bmatrix} -9.65351832 \cdot 10^{-4} & -5.97487759 \cdot 10^{-5} \\ 7.04023281 \cdot 10^{-4} & -7.10867350 \cdot 10^{-5} \\ 2.27013489 \cdot 10^{-3} & 4.45169794 \cdot 10^{-4} \\ 6.27266485 \cdot 10^{-3} & 5.02188425 \cdot 10^{-4} \end{bmatrix}, \\
 C &= [-525.06454659 \quad -72.35579091 \quad 26.45634838 \quad -35.48394308],
 \end{aligned} \tag{17}$$

Note that in two MPC formulations (MPC1 and MPC2) where the inlet HCl concentration C_{HCl}^{SMP1} is not considered as measurable disturbance, the input model matrix is reduced, that is, $\tilde{B} = B$. We underline that the system (17) is always used as the simulated process, i.e., for the FFT simulation, and also as model adopted by the MPC formulations, that is, MPC1-md and MPC2-md have no plant-model mismatch.

The controller tuning. For the simulation of the feedback PI controller, the following parameters were set: $PB = 0.025$, $TI = 30$ min, while for the feed-forward component, $r_s = 1$ and $R_{s_f} = 3.98$ were used. Note

that this set of parameters was actually adopted on the WtE plant in that period of data collection. The specific values were obtained in the past via standard step tests by plant operators.

For the different MPC formulations, parameters were tuned after a suitable trial-error approach. For the static module, values are always the same: $\bar{Q} = 100$, $\bar{R} = 0$. For the dynamic module, the following penalty values were adopted: $Q = 10 I_{n_x}$, $S = 0.05$, $R = 0.05$ when present, and the terminal penalty matrix Q_N is calculated with the Algebraic Riccati Equation, thus depending on the matrices A, B, Q , and S . The following constraints are imposed: 0–300 kg/h for the manipulated variable, that is, $Q_{Ca(OH)_2}$; 0–600 mg/Nm³ for the controlled variable, i.e., C_{HCl}^{SMP2} .

4.2. Results discussion

A first comparison of the different control structures is reported in Fig. 6, where input and output variables for FFT, MPC1 and MPC1-md are reported in two first panels. The bottom panel shows the input concentration of HCl: the real measured values at SMP1 is displayed just for comparison with the two disturbance estimate (\hat{d}) used within the MPC model. It is obvious noting that MPC1-md, which exploits the actual level of inlet HCl, yields a null estimate of the disturbance, since no plant-model mismatch is present. Recalling what anticipated in Section 3, we underline how the disturbance model estimate \hat{d}_k^* in MPC1 is not exactly matching the real process disturbance (C_{HCl}^{SMP1}), even though the only mismatch between the controller model and the simulated process is represented by $d_{m,k}$. This is particularly visible in Fig. 6 in the first part of the time window: the initial value of \hat{d}_k^* , i.e., \hat{d}_0^* , is zero, while at the same time $d_{m,0} \approx 900$ mg/Nm³. Then, with the estimator update and filtering, \hat{d}_k^* is reaching the mean value of $d_{m,k}$ in a few time steps, introducing a one-step delay of the control action.

Moreover, it is evident how the two considered MPC formulations (MPC1 and MPC1-md, both with the dynamic module as in (12)) outperform the simulation of the actual control system (FFT). The advanced controllers ensure a closer set-point tracking ($C_{HCl,SP}^{SMP2} = 450$ mg/Nm³), and, at the same time, require a lower dosage of Ca(OH)₂. This effective behavior solves the trade-off between compliance of emission limits at the stack and reduced solid residues at the first baghouse. In particular, it is worth noting how the MPC architectures impose a close-to-zero value of dry sorbent in the time interval 100:300 min, when the input HCl concentration is particularly low. The mean concentration in this time window is indeed much lower (≈ 740 mg/Nm³) than the mean level registered in the whole data set (≈ 980 mg/Nm³). The simulated FFT controller implies always a higher dosage, typically

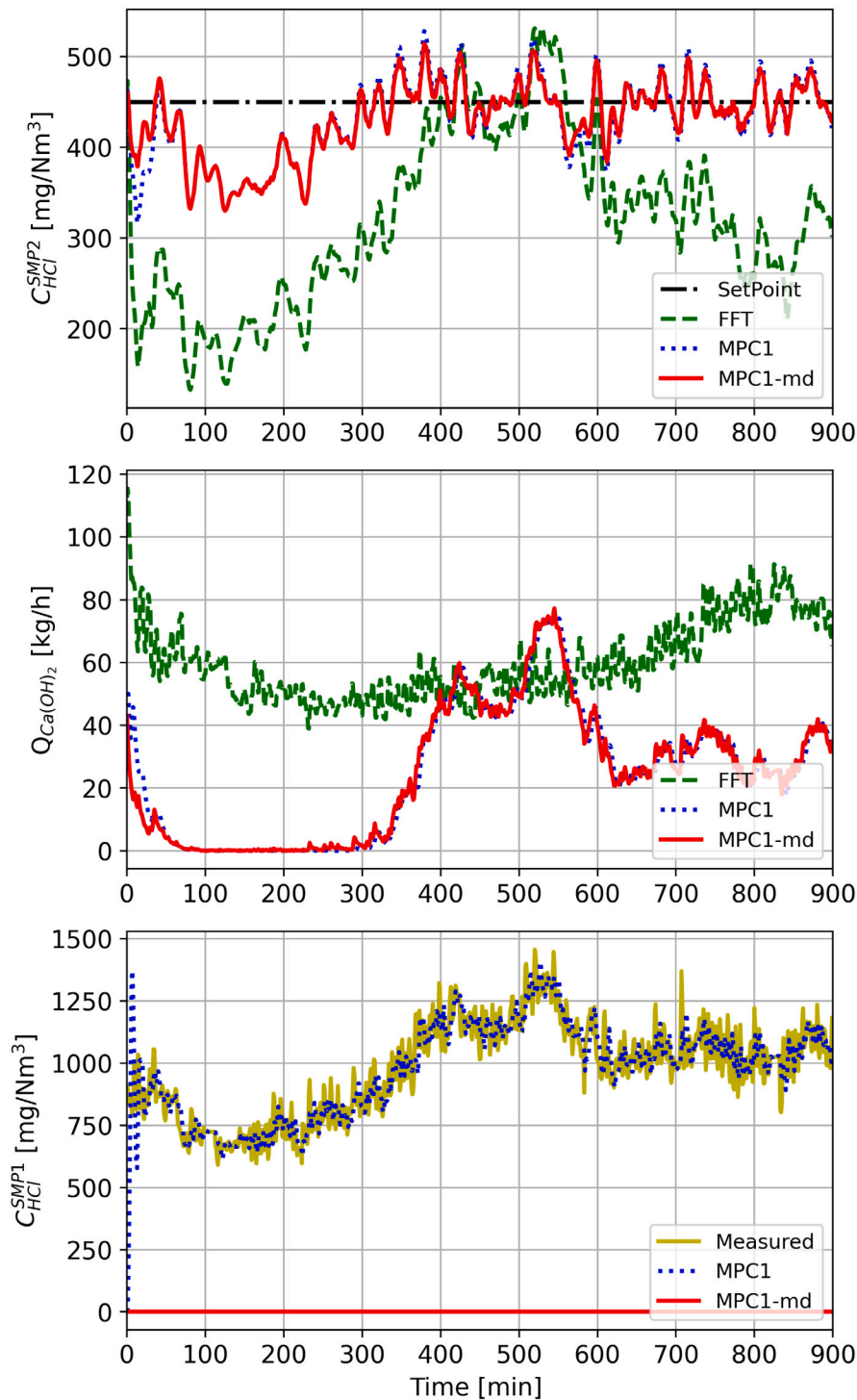


Fig. 6. FFT vs. MPCs formulations, considering or not C_{HCl}^{SMP1} as measurable disturbance.

more than 39 kg/h, with a mean value of 60 kg/h; whereas, average sorbent flow rate for MPC controllers is around 24–25 kg/h.

Key performance indicators. To better quantify the performance of the five controllers under comparison, the following three key performance indicators (KPI) are defined:

$$TSD = \sum_{k=0}^{N_s-1} Q_{Ca(OH)_2} T_s \quad (18)$$

$$IAE = \sum_{k=0}^{N_s-1} |e_k| T_s \quad (19)$$

$$TSV = \sum_{k=0}^{N_s-1} |Q_{Ca(OH)_2,k+1} - Q_{Ca(OH)_2,k}| T_s \quad (20)$$

The Total Sorbent Dosage (TSD) evaluates the amount of dosed hydrated lime $Ca(OH)_2$ in the analyzed time interval; the IAE index is the classical integral of absolute error. Finally, the Total Sorbent Variation (TSV) considers the absolute difference between two consecutive amounts of dosed $Ca(OH)_2$, and it is related to the mechanical stress of the screw feeder.

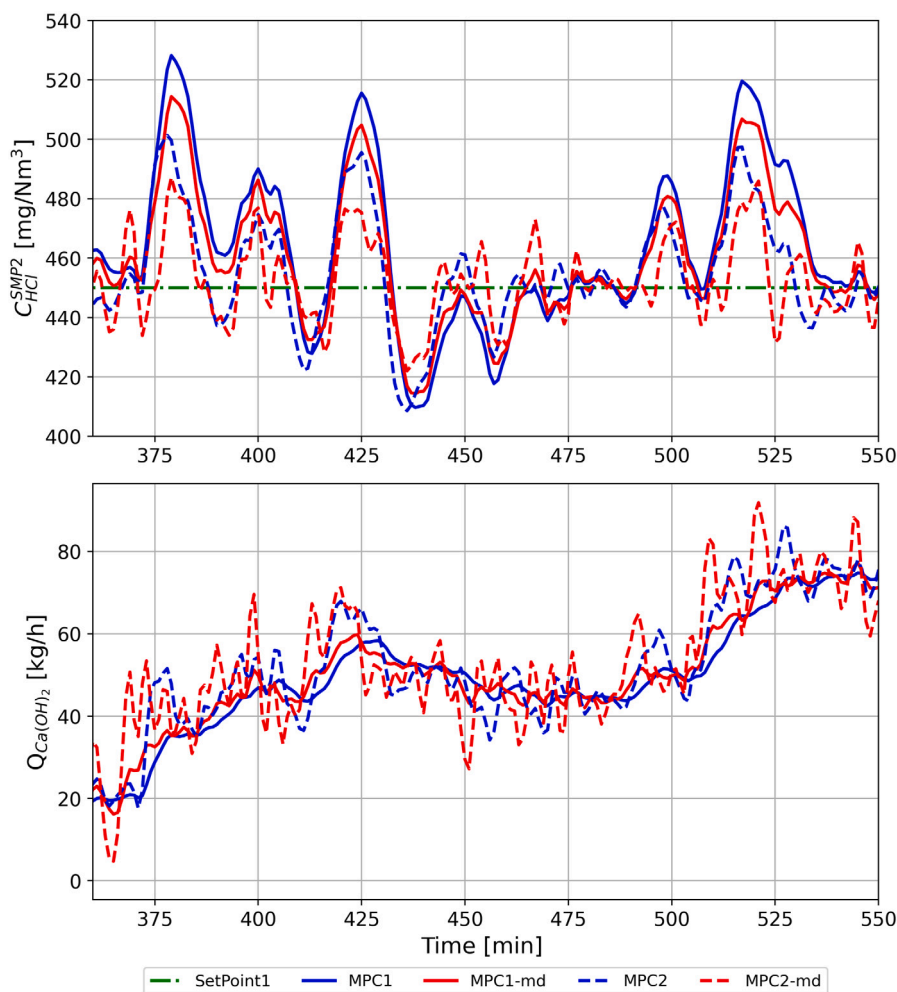


Fig. 7. Behavior of different MPC formulations in the time window 360:550: C_{HCl}^{SMP2} (top) and $Q_{Ca(OH)_2}$ (bottom).

Table 1

Comparing different control systems in terms of key performance indicators.

Controller	FFT	MPC1	MPC1-md	MPC2	MPC2-md
TSD [kg]	899.96	373.76	370.37	369.20	369.09
IAE	$124.5 \cdot 10^3$	$33.42 \cdot 10^3$	$29.54 \cdot 10^3$	$27.11 \cdot 10^3$	$23.80 \cdot 10^3$
TSV [kg]	30.61	8.27	13.33	31.18	59.25

Results for the three considered KPIs are summarized in Table 1. For the sake of clarity, the behavior of MPC2 and MPC2-md are not shown in Fig. 6, albeit their performance have still been evaluated and are shown in Table 1. It is confirmed how the various MPC formulations outperform the simulated FFT control system.

In particular, very lower values of TSD index are registered, which correspond to savings of around 60% of $Ca(OH)_2$ dosage. At the same time, the four advanced controllers guarantee a closer set-point tracking, since reductions in terms of IAE index are around 74–82%.

A clearer visualization of the different behaviors of the four investigated MPC solutions is shown in Fig. 7; note that a selected time window (360:550 min) is considered with the set-point (450 mg/Nm³) just for the sake of clarity in the picture. All MPC solutions are very similar, but some distinctions can be made. As a matter of fact, further advantages are obtained by using the improved dynamic optimization problem (13). In details, when also R matrix is adopted, both TSD and IAE decrease; this effect can be observed when passing from MPC1 to MPC2, and also from MPC1-md to MPC2-md. This result can be explained by considering that formulation of (13) is suited to

weigh also the input deviations from the target values, thus minimizing the input values to its lower bound. Further advantages are obtained when the measurable disturbance is included in the model formulation. Again, both TSD and IAE are reduced by MPC1-md with respect to MPC1, and by MPC2-md with respect to corresponding MPC2. It is clear that such improvement in the first two KPIs values is at the expense of higher input oscillations, which are not always acceptable from a technical point of view. As a matter of fact, the TSV value is decreasing using the tuning formulation of MPC1, while is much higher for MPC2 in which also the distance of the input from its target is weighted. Therefore, it is clear that a controller imposing less variable sorbent rates can be preferred as it induces less mechanical stress on the feeding system.

A brief economic assessment is here reported. By referring to values of Table 1, for the four proposed MPC formulations, a mean value of total sorbent dosage $\overline{TSD} = 370.6$ kg is obtained, which is around 40% of the dosage (≈ 900 kg) required by the FFT controller. Thus, a reduction of 530 kg of solid sorbent is possible; by considering a price for $Ca(OH)_2$ of 0.3 €/kg, an economic benefit of around 160 € is obtained. This saving is obtained in just 900 min (15 h) of operation of the treatment unit; this means (more than) 10 € per hour. For an annual operation period of 8200 h, the saving guaranteed by an MPC solution can be estimated into at least 82,000 €. Note that this analysis does not consider the reduced wear of the actuation system (that is, the screw feeder), which can be quantified by the total variation of sorbent dosage (TSV), and mostly the savings related to the reduced residual calcium chemicals to be further treated or disposed, which is an aspect beyond the scope of the present work.

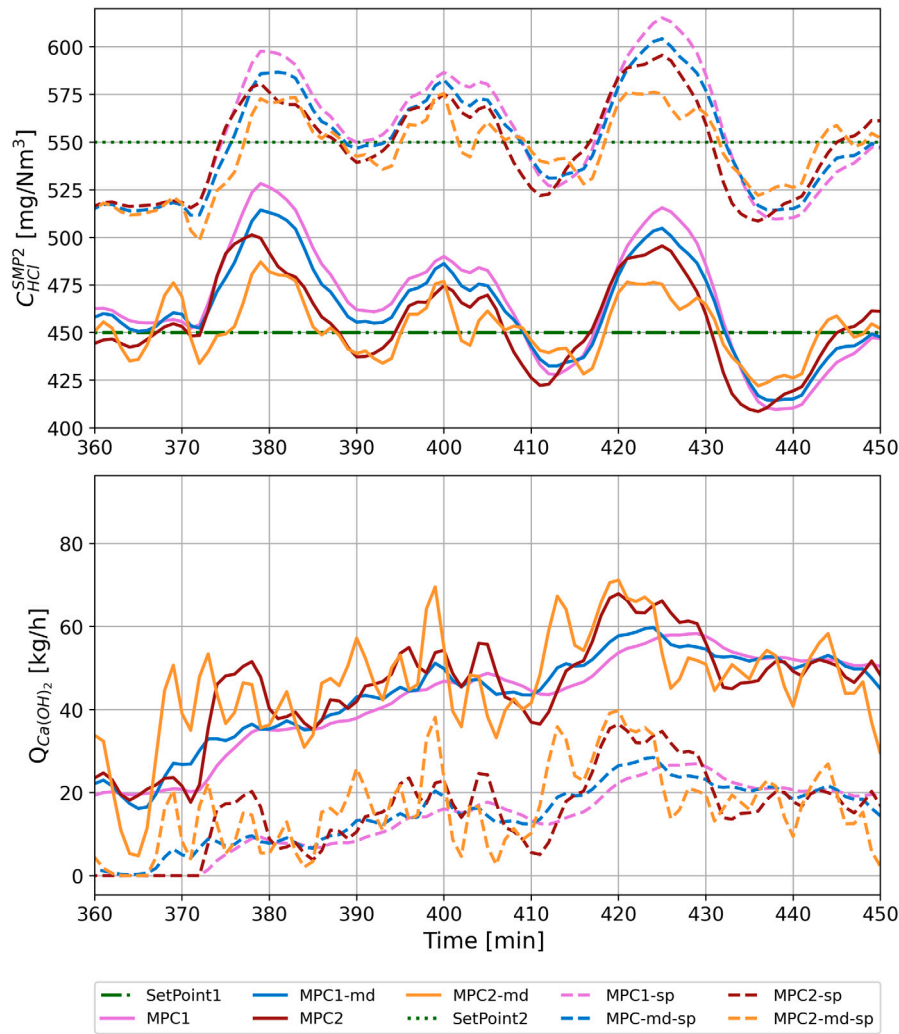


Fig. 8. Behavior of different MPC formulations for two different set-points. The suffix “sp” stands for the higher set-point trends.

Different operating conditions. Another aspect involves the investigation of the various MPC formulations for different operating conditions. As a matter of fact, and as already anticipated in Section 2, the set-point imposed on the FFT architecture is ensuring compliance with emission limits at the stack by considering also the high range of performance variability that such a controller can guarantee. Nonetheless, the MPC algorithm is able to maintain a closer value of the controlled variable C_{HCl}^{SMP2} around its set-point. This means that if a higher set-point is adopted, first the concentration of HCl exiting the baghouse at SMP2 is higher, but still more stable around its newly imposed value, and second the required dosage of $Ca(OH)_2$ can be much lower improving the abatement process both economically and environmentally. In particular, the new set-point considered for this test is 550 mg/Nm^3 .

The effect of the two different dynamic objective functions and the inclusion of measurable disturbance in the model is thus investigated. For both set-point values, it is worth noting how the performance is different in terms of set-point tracking and reduced sorbent dosage by: (i) adopting both S and R matrices in the dynamic module, e.g., passing from MPC1 to MPC2 and from MPC1-md to MPC2-md, and (ii) by exploiting the measurable disturbance within the model process, that is, passing from MPC1 to MPC1-md and from MPC2 to MPC2-md. For example, aggressive behaviors are registered for MPC2 and MPC2-md solutions, that is, when considering the R matrix in the dynamic module, which means that also the input deviations from the target values are weighted.

The effect of the higher set-point (550 mg/Nm^3) is shown in Fig. 8 where only a selected time window (360:450 min) is displayed for the sake of clarity. The main result to be underlined is how the higher setpoint implies an almost complete homogeneous shift of the trends calculated at 450 mg/Nm^3 . This is easily explained considering that both the controller model and the simulated systems are linear, that is, any nonlinearity possibly present in the real industrial scenario is here not considered. The main difference between the trends at the two set-points can be seen in the first part of the plot (360:380 min) in which the amount of HCl entering the abatement system (C_{HCl}^{SMP1}) is already lower than 550 mg/Nm^3 that the corresponding manipulated variable ($Q_{Ca(OH)_2}$) is set to zero for MPC1-sp and MPC2-sp.

A quantitative assessment is performed also for the higher set-point condition. Results for the three considered KPI are summarized in Table 2. All MPC solutions perform similarly, but once again some distinctions are due: lower TSD and IAE are confirmed by using the problem (13) in the dynamic module; by including the measurable disturbance within the model formulation, IAE index again decreases, while TSD is higher. Finally, higher TSV value, that is, aggressive behavior, are registered when considering R matrix, that is, when moving from MPC1 to MPC2 and from MPC1-md to MPC2-md, and also when the measurable disturbance is exploited, i.e., from MPC1 to MPC1-md and from MPC2 to MPC2-md. Moreover, by comparing the values of Table 1 obtained for the low set-point scenario with corresponding numbers of Table 2, it is clear how increasing the set-point of outlet HCl concentration allows a remarkable reduction of dry sorbent amount.

Table 2

Comparing different MPC formulations in terms of key performance indicators (higher set-point condition, $C_{HCl,sp}^{MPC1} = 550 \text{ mg/Nm}^3$).

Controller	MPC1	MPC1-md	MPC2	MPC2-md
<i>TSD</i> [kg]	106.32	109.72	97.24	103.92
<i>IAE</i>	$65.74 \cdot 10^3$	$64.06 \cdot 10^3$	$60.73 \cdot 10^3$	$59.98 \cdot 10^3$
<i>TSV</i> [kg]	5.45	8.85	17.82	33.74

Lower values of *TSD* are obtained by every MPC formulation with respect to the corresponding lower set-point scenario. Nevertheless, set-point tracking capabilities are still guaranteed, as shown by the values of *IAE* index. Moreover, the input variations recorded with *TSV* are still acceptable. Finally, it is evident how the high set-point condition implies that a larger HCl concentration is fed to the reaction tower of the second treatment stage, hence, a higher dosage of NaHCO_3 is required with relative higher cost of disposal of solid sodium residues. Note that an optimization of both stages is out of the scope of the present paper and will be object of future research, where a larger process model will be identified and adopted, and further enhanced MPC formulations may be evaluated.

5. Conclusion/outlook

The management of acid gas removal units of waste-to-energy facilities proves to be an interesting and challenging control problem, as traditional control schemes are destabilized by the volatility and amplitude of process disturbances. In particular, major issues arise in the first stage of abatement, where Ca(OH)_2 is dosed to reduce HCl content of the acid flue gas. The present study has involved a two-stage dry sorbent system within an Italian treatment plant, and the benefits given by advanced control structures with respect to the current sub-optimal control architecture are illustrated.

Using a state-space model, previously identified and tested, four different model predictive control solutions were derived and applied to routine data to increase the process performance. A solid profit-safety trade-off was achieved: a strict set-point tracking on outlet HCl concentration and, at the same time, minimal sorbent levels and then minimal solid residues were registered, and also limited stress to the actuation system was possible. The formulated MPCs outperformed the simulated actual control logic by requiring 60% less in terms of the sorbent dosage (saving at least 80,000 €/year) and allowing smoother management of the sorbent feeding system by imposing bound limits on its rate-of-change (with a maximum reduction of 70%). Combining optimal control subject to constraints fulfillment and a data-driven model allows to better forecast the sorbent flow rate required avoiding the sudden spikes that the basic control operation needs. Further advantages in terms of set-point control and sorbent dosage are obtained by using an improved dynamic optimization problem, and also when the measurable disturbance is included in the model formulation, but higher stress on the actuation system is registered.

Clearly, the proposed solution is a promising update on the current control logic but further studies have to be performed specifically evaluating the computational costs involved for an online implementation in the facility. In addition, future works will also focus on the second treatment stage, where HCl concentration is further reduced by dosing NaHCO_3 . Finally, as explained when describing the treatment plant, HCl is not the only acid gas to be removed, therefore modeling the sulfur content in the flue gas is also to be considered when aiming at fully improving the management of the WtE treatment unit.

CRedit authorship contribution statement

Riccardo Bacci di Capaci: Methodology, Software, Formal analysis, Writing. **Marco Vaccari:** Methodology, Software, Formal analysis, Writing, Validation. **Gabriele Pannocchia:** Methodology, Validation, Supervision.

Declaration of competing interest

The authors declare that they have no known competing financial interests or personal relationships that could have appeared to influence the work reported in this paper.

Data availability

The data that has been used is confidential.

Acknowledgments

This work was possible thanks to the previous collaboration with people of the Department of Civil, Chemical, Environmental and Material Engineering, University of Bologna, Italy. We do thank Prof.s Alessandro Dal Pozzo, Giacomo Antonioni, and Valerio Cozzani for the fruitful discussions and sharing of process information and data of the Waste-to-Energy plant under study.

References

- Armenise, G., Vaccari, M., Bacci di Capaci, R., Pannocchia, G., 2018. An open-source system identification package for multivariable processes. In: 2018 UKACC 12th International Conference on Control. CONTROL, IEEE, pp. 152–157.
- Auger, F., Hilairet, M., Guerrero, J.M., Monmasson, E., Orłowska-Kowalska, T., Katsura, S., 2013. Industrial applications of the Kalman filter: A review. IEEE Trans. Ind. Electron. 60 (12), 5458–5471.
- Bacci di Capaci, R., Pannocchia, G., Dal Pozzo, A., Antonioni, G., Cozzani, V., 2022. Data-driven models for advanced control of acid gas treatment in waste-to-energy plants. IFAC-PapersOnLine 55 (7), 869–874, 13th IFAC Symposium on Dynamics and Control of Process Systems, including Biosystems DYCOPS 2022.
- Biganzoli, L., Racanella, G., Rigamonti, L., Grosso, M., 2015. High temperature abatement of acid gases from waste incineration. Part II: Comparative life cycle assessment study. Waste Manag. 35, 127–134.
- Bigoni, D., Benaglia, R., Galligani, T., Stancari, S., Calderara, S., 2021. Robust control of a waste-to-energy facility. In: Proceedings of SIMAI 2020+21.
- Chan, L.L.T., Chen, J., 2018. Improving the energy cost of an absorber-stripper CO_2 capture process through economic model predictive control. Int. J. Greenh. Gas Control 76, 158–166.
- Dai, M., Yu, Z., Tang, Y., Ma, X., 2020. HCl emission and capture characteristics during PVC and food waste combustion in CO_2/O_2 atmosphere. J. Energy Inst. 93 (3), 1036–1044.
- Dal Pozzo, A., Abagnato, S., Cozzani, V., 2023. Assessment of cross-media effects deriving from the application of lower emission standards for acid pollutants in waste-to-energy plants. Sci. Total Environ. 856, 159159.
- Dal Pozzo, A., Guglielmi, D., Antonioni, G., Tugnoli, A., 2018a. Environmental and economic performance assessment of alternative acid gas removal technologies for waste-to-energy plants. Sustain. Prod. Consumpt. 16, 202–215.
- Dal Pozzo, A., Lazazzara, L., Antonioni, G., Cozzani, V., 2020. Techno-economic performance of HCl and SO_2 removal in waste-to-energy plants by furnace direct sorbent injection. J. Hard Mater. 394, 122518.
- Dal Pozzo, A., Moricone, R., Antonioni, G., Tugnoli, A., Cozzani, V., 2018b. Hydrogen chloride removal from flue gas by low-temperature reaction with calcium hydroxide. Energy Fuels 32 (1), 747–756.
- Dal Pozzo, A., Muratori, G., Antonioni, G., Cozzani, V., 2021. Economic and environmental benefits by improved process control strategies in HCl removal from waste-to-energy flue gas. Waste Manag. 125, 303–315.
- EU-Eurostat, 2021. Municipal waste statistics. data retrieved from Municipal waste statistics, https://ec.europa.eu/eurostat/statistics-explained/index.php?title=Municipal_waste_statistics.
- Hossein Sahraei, M., Ricardez-Sandoval, L., 2014. Controllability and optimal scheduling of a CO_2 capture plant using model predictive control. Int. J. Greenh. Gas Control 30, 58–71.
- Iqbal, M.W., Kang, Y., 2021. Waste-to-energy supply chain management with energy feasibility condition. J. Clean. Prod. 291, 125231.
- Kuo, P.-C., Illathukandy, B., Kung, C.-H., Chang, J.-S., Wu, W., 2021. Process simulation development of a clean waste-to-energy conversion power plant: Thermodynamic and environmental assessment. J. Clean. Prod. 315, 128156.
- Leskens, M., van Kessel, L., Bosgra, O., 2005. Model predictive control as a tool for improving the process operation of MSW combustion plants. Waste Manag. 25 (8), 788–798.
- Li, Y., Dai, J., Cui, L., 2020. The impact of digital technologies on economic and environmental performance in the context of industry 4.0: A moderated mediation model. Int. J. Prod. Econ. 229, 107777.
- Makarichi, L., Jutidamrongphan, W., Techato, K., 2018. The evolution of waste-to-energy incineration: A review. Renew. Sustain. Energy Rev. 91, 812–821.

- Mousavi, S.A., Hafezalkotob, A., Ghezavati, V., Abdi, F., 2021. An integrated framework for new sustainable waste-to-energy technology selection and risk assessment: An R-TODIM-R-MULTIMOOSRAL approach. *J. Clean. Prod.* 130146.
- Ni, T., Si, J., Lu, F., Zhu, Y., Pan, M., 2022. Performance analysis and optimization of cascade waste heat recovery system based on transcritical CO₂ cycle for waste heat recovery in waste-to-energy plant. *J. Clean. Prod.* 331, 129949.
- Pannocchia, G., 2015. Offset-free tracking MPC: A tutorial review and comparison of different formulations. In: 2015 European Control Conference. ECC, IEEE, pp. 527–532.
- Pannocchia, G., Calosi, M., 2010. A predictor form PARSIMonious algorithm for closed-loop subspace identification. *J. Process Control* 20 (4), 517–524.
- Pavlas, M., Touš, M., Bébar, L., Stehlfk, P., 2010. Waste to energy - An evaluation of the environmental impact. *Appl. Therm. Eng.* 30 (16), 2326–2332.
- Putna, O., Janoš'ák, F., Pavlas, M., 2020. Greenhouse gas credits from integrated waste-to-energy plant. *J. Clean. Prod.* 270, 122408.
- Shiek, A.G., Machavolu, V.R.K., Seepana, M.M., Ambati, S.R., 2021. Design of control strategies for nutrient removal in a biological wastewater treatment process. *Environ. Sci. Pollut. Res.* 28, 12092–12106.
- Shin, Y., Smith, R., Hwang, S., 2020. Development of model predictive control system using an artificial neural network: A case study with a distillation column. *J. Clean. Prod.* 277, 124124.
- Skupin, P., aszczyk, P., Goud, E.C., Vooradi, R., Ambati, S.R., 2022. Robust nonlinear model predictive control of cascade of fermenters with recycle for efficient bioethanol production. *Comput. Chem. Eng.* 160, 107735.
- Vaccari, M., Pannocchia, G., Tognotti, L., Paci, M., Bonciani, R., 2020. A rigorous simulation model of geothermal power plants for emission control. *Appl. Energy* 263, 114563.
- Wu, X., Shen, J., Li, Y., Wang, M., Lawal, A., 2018. Flexible operation of post-combustion solvent-based carbon capture for coal-fired power plants using multi-model predictive control: A simulation study. *Fuel* 220, 931–941.
- Wu, X., Wang, M., Liao, P., Shen, J., Li, Y., 2020. Solvent-based post-combustion CO₂ capture for power plants: A critical review and perspective on dynamic modelling, system identification, process control and flexible operation. *Appl. Energy* 257, 113941.
- Xu, Q., Hao, X., Shi, X., Zhang, Z., Sun, Q., Di, Y., 2022. Control of denitration system in cement calcination process: A novel method of deep neural network model predictive control. *J. Clean. Prod.* 332, 129970.
- Zhang, Q., Turton, R., Bhattacharyya, D., 2018a. Nonlinear model predictive control and H robust control for a post-combustion CO₂ capture process. *Int. J. Greenh. Gas Control* 70, 105–116.
- Zhang, H., Yu, S., Shao, L., He, P., 2019. Estimating source strengths of HCl and SO₂ emissions in the flue gas from waste incineration. *J. Environ. Sci.* 75, 370–377.
- Zhang, K., Zhao, J., Zhu, Y., 2018b. MPC case study on a selective catalytic reduction in a power plant. *J. Process Control* 62, 1–10.